Journal of Power Sources 362 (2017) 219–227

Contents lists available at ScienceDirect

Journal of Power Sources

journal homepage: www.elsevier.com/locate/jpowsour

Enhancement of thermal transport in Gel Polymer Electrolytes with embedded BN/Al_2O_3 nano- and micro-particles

Vivek Vishwakarma, Ankur Jain*

Mechanical and Aerospace Engineering Department, University of Texas at Arlington, Arlington, TX, USA

HIGHLIGHTS

- Measures thermal transport properties of Gel Polymer Electrolytes (GPEs).
- Investigated effect of inclusion of BN/Al_2O_3 ceramic nano/microparticles.
- Results indicate substantial improvement in thermal transport.
- Experimental measurements are in good agreement with theoretical model.
- Results may help understand thermal and ionic transport trade-offs in GPEs.

ARTICLE INFO

Article history:
Received 16 May 2017
Received in revised form
5 July 2017
Accepted 11 July 2017
Available online 19 July 2017

Keywords:
Gel Polymer Electrolyte
Li-ion battery
Nanoparticles
Thermal transport
Battery safety

ABSTRACT

While Gel Polymer Electrolytes (GPEs) have been widely investigated for use in next-generation Li-ion cells due to the potential for improved thermal safety, thermal transport within a GPE is still poorly understood. Among all materials in a Li-ion cell, the GPE has the lowest thermal conductivity, and hence determines the overall rate of heat flow in a Li-ion cell. This makes it critical to measure and understand thermal transport in a GPE and investigate trade-offs between thermal and ionic transport. This paper presents measurements of thermal and ionic conductivities in a PVdF-based GPE. The effect of incorporating BN/Al_2O_3 ceramic nano/microparticles in the GPE on thermal and ionic transport is characterized. Measurements indicate up to 2.5X improvement in thermal conductivity of activated GPE membranes, with relatively minor effect on electrochemical performance of GPE-based single-layer cells. The measured enhancement in thermal conductivity is in very good agreement with theoretical calculations based on the effective medium theory that accounts for thermal transport in a dispersed, two-phase medium such as a GPE. The fundamental insights gained in this work on thermal transport in a GPE and the role of nano/microparticle inclusions may facilitate thermal-electrochemical optimization and design of GPEs for safe, high-performance Li-ion cells.

1. Introduction

Li-ion batteries have been used extensively for energy storage and conversion in electric vehicles, grid storage systems, portable electronics, etc. due to their excellent electrochemical performance [1–3]. New battery paradigms are beginning to emerge to overcome the limitations of present Li-ion cells and extend the state-of-the-art for performance and safety. For example, the use of volatile and combustible liquid electrolyte in traditional Li-ion cells poses a severe risk of fire and explosion [4,5], even at slightly elevated cell temperature. Such safety concerns have severely restricted the performance envelope of Li-ion cells. Traditional Li-ion cells also suffer from significant design restrictions due to the use of liquid electrolyte and rigid separator membranes. In the recent past, gel polymer electrolytes (GPEs) have been widely investigated as a potential replacement of the conventional liquid electrolyte and separator [6–9]. A GPE comprises a polymer matrix capable of holding liquid electrolyte without sacrificing much of the electrochemical and mechanical performance [9]. The absorbed liquid electrolyte is immobilized within the pores of the polymer matrix, retaining the properties of the liquid electrolyte and conventional separator, while minimizing the volume of the combustible electrolyte needed, which results in improved safety [7]. By eliminating the need to enclose a liquid electrolyte in a rigid containment, GPEs

* Corresponding author. 500 W First St, Rm 211, Arlington 76019, TX, USA.
E-mail address: jaina@uta.edu (A. Jain).

http://dx.doi.org/10.1016/j.jpowsour.2017.07.035
0378-7753/

also offer an added advantage of enabling batteries in a wide variety of shapes, including flexible batteries [10,11]. Polyethylene oxide (PEO), polyacrylonitrile (PAN), polymethyl methacrylate (PMMA), and polyvinylidene fluoride (PVdF) are the most widely studied polymer matrices for GPEs [7,9]. The electrochemical performance of GPE-based Li-ion cells has been studied to understand the effect of replacing the traditional separator with a GPE. For example, GPE based Li–ion cells have been tested for charge-discharge cycling and capacity fade [13–20]. Cycling performance of a $LiCoO_2$/GPE/Anode cell between 2 and 4.2 V has been investigated, showing stable charge/discharge performance for up to 50 cycles without significant capacity loss and good compatibility of the polymer electrolyte with electrode materials [14–22]. The capacity fade in an Al_2O_3/$BaTiO_3$ ceramic filler based Li-ion polymer cell has been shown to be less than 10% after 50 discharge cycles [19]. While several research challenges remain, GPEs offer a plausible alternative to liquid electrolytes in next-generation electrochemical batteries [12,21].

A key question that continues to be investigated is the effect of using a GPE on various transport and storage processes, such as charge transport and capacity. PVdF based polymer membranes offer high dielectric constant, thereby increasing charge carrying capacity [23]. The semi-crystalline structure of PVdF also helps in enhanced ion storage and mobility [23]. When used along with a mixture of carbonate esters such as Ethylene Carbonate (EC) and Propylene Carbonate (PC), PVdF has been shown to offer reasonably large ionic conductivity of around 2 mS/cm [23,24]. In order to further increase the ionic conductivity of a GPE, the use of ionic liquids such as imidazolium cations in the liquid electrolyte has been widely studied [25,26]. The use of 1-ethyl-3-methylimidazolium tetrafluoroborate ($EMIBF_4$) as an electrolyte solvent for $LiBF_4$ has been shown to result in ionic conductivity in the 0.23–10 mS/cm range between 20 and 40 °C [26]. The fundamental nature of Li ion transport phenomena in the presence of these ionic liquids continues to be a topic of much current interest [17,27].

In addition to ionic transport, thermal transport in GPE materials is also important to study. Although the use of a GPE in a Li-ion cell reduces the volume of combustible electrolyte, it also leads to introduction of new materials and manufacturing processes. Several research challenges related to thermal transport in GPEs must be fully understood before the safety advantage of GPEs can be conclusively established [12,21]. The fundamental nature of heat transfer through GPE materials is still poorly understood, with very limited experimental data on fundamental thermal transport properties. The dominance of interfacial thermal contact resistance between electrode and separator in thermal transport in a conventional Li-ion cell [28] may not hold for a GPE based cell due to the distinctly different manufacturing and assembly of a GPE-based cell. Since electrode material is directly deposited on a GPE [29], interfacial thermal contact resistance may be negligible, and therefore, heat transfer through the GPE may be the slowest, rate-determining step in overall thermal conduction process inside a Li-ion cell. This makes it critical to experimentally characterize the thermal transport properties of a GPE, and explore mechanisms for thermal transport enhancement. While some work is available on thermal characterization of traditional separators, including thermal conductivity [30,31] and interfacial thermal contact resistance [28] measurements, there is a lack of such work on GPE materials.

Impregnation of micro-sized and nano-sized ceramic fillers has been used extensively for enhancement of mechanical, electrical, thermal and multifunctional properties in polymers [19,32–35]. However, this approach has not yet been investigated much in the context of thermal transport in GPEs. Some work has been carried out with ceramics fillers such as Al_2O_3 [19,32,36–39], $BaTiO_3$ [19] and TiO_2 [19] in a GPE to investigate electrochemical stability, ionic conductivity and compatibility with electrodes. Recently, thermally conductive Al_2O_3/polymer composite separator has been developed by mixing PVdF-HFP and nano-micro sized Al_2O_3 particles for conventional Li-ion batteries [32]. Clearly, much more needs to be done to fully understand the effect of nano/micro-sized particle inclusion on the thermal properties of GPEs, and eventually on thermal performance of GPE-based Li-ion cells.

This paper presents measurement and enhancement of thermal transport in PVdF-based GPEs through Al_2O_3 and BN ceramic nano/micro particle inclusion in the GPE. Measurements show 13X and 2.5X improvement in thermal conductivity of the PVdF membrane and PVdF based GPE respectively. Experimental results are found to be in good agreement with the effective medium theory (EMT) model for thermal conductivity of baseline and thermally enhanced GPEs. Implications of such nano/microparticle inclusion on the electrochemical performance of the GPE and GPE-based Li-ion cell is also reported. Electrochemical impedance spectroscopy (EIS) and charge-discharge measurements characterize the effect of nanoparticle inclusion on electrochemical performance, highlighting the need for careful consideration of thermal-electrochemical trade-offs in GPEs. Results presented here may help understand and enhance thermal transport in GPE materials. The thermal transport properties reported in this work may facilitate accurate simulations of thermal performance and safety of GPE-based Li-ion cells, as well as multiphysics thermal-electrochemical co-optimization.

2. Experimental methods and materials

2.1. Materials

Al_2O_3 and BN nanoparticles (800 nm) and BN micro particles (~2.5 μm) (US Research Nanomaterials Inc.) are used in this work for investigating GPE thermal enhancement. These materials are known to offer high thermal conductivity of 18–34 W/mK [32], high electrical resistivity of around 10^{14} Ω-cm, light weight and moderate cost compared to other ceramics [19,35,36,40–42], which is critical for a GPE. Poly(vinylidene Fluoride) (PVdF) (Sigma Aldrich) is used as the gel polymer host matrix. PVdF offers high dielectric constant, supports high charge concentration and offers high thermal stability, due to which it has been used widely as the polymer host material for Li-ion battery GPEs [43,44]. Lithium hexafluorophosphate ($LiPF_6$) (Sigma Aldrich) is used as the electrolyte due to its excellent ionic conductivity in carbonate based solvents [44]. 1-Methyl-2-pyrrolidone (NMP) (Sigma Aldrich) is used as a solvent to dissolve PVdF and obtain porous membranes. NMP offers high boiling point, low volatility and non-toxicity [45]. A mixture of ethylene carbonate (EC) (Sigma Aldrich) and propylene carbonate (PC) (Sigma Aldrich) acts as plasticizer for PVdF and is used to extract gel polymer membranes. Also, EC/PC ester acts as a solvent for $LiPF_6$ and offers thermal stability [46]. 1-Ethyl-3-methylimidazolium triluoromethanesufonate (EMI-TF) (Sigma Aldrich) is also used as a part of the ionic liquid in the electrolyte mixture. EMI-TF offers very high ionic conductivity (10 mS/cm), which has been reported to enhance the overall ionic conductivity of the electrolyte mixture [16,47].

2.2. GPE synthesis and enhancement

The synthesis of 100–1200 μm thick PVdF-based polymer membranes is carried out by following a previously described procedure [43]. The porous PVDF membrane is obtained by first making an ester solution of 1:1 mixture of EC and PC by mass, and heating at 80 °C (Isotemp, Fisher Scientific) until a clear solution is obtained. This ester solution is then mixed with NMP and PVdF in

40%, 44% and 16% proportion by weight respectively, as shown in Fig. 1(A). The mixture is heated at 110 °C (Isotemp, Fisher Scientific) and stirred until a pale viscous solution is obtained. This solution is poured in petri dishes (Fig. 1(B)) and baked at 80 °C in 0.07 MPa vacuum in a vacuum oven (Across International AccuTemp-09) for 2 h.

The membranes are then soaked in 10% ethanol for 8 h. Finally, the GPE is obtained by soaking and activating the PVdF membrane in a mixture of 1.0 M $LiPF_6$ with ionic liquid solvents (2:1:1 by volume of EMI-TF, EC and PC) for 24 h. For samples with nano/microparticle inclusion, the nano/microparticles are mixed with NMP during the PVdF membrane formation process. 100–1200 μm thick samples of 4 × 4 cm^2 size are obtained through this process (Fig. 1(C)). The thickness of the membranes is controlled through the volume of the solution poured in petri dishes, and measured using vernier calipers (±10 μm) (Fig. 1(D)). The resulting PVdF based membranes are highly porous in nature, as shown in Supplementary Fig. S1(A), with pore diameter ranging from 2 to 10 μm and PVdF grain diameter ranging from 2 to 5 μm. Fig. 1(E) and (F) show SEM images of the porous PVdF membrane with no nanoparticle and with 800 nm BN nanoparticles respectively. Fig. 1(F) shows that BN nanoparticles are bonded uniformly to the outer periphery of the PVdF grains. Some agglomeration is observed at higher nanoparticle concentration. Tables 1 and 2 summarize GPE samples with a variety of micro/nanoparticles concentration investigated in this work. In addition to the baseline case without any nano/microparticles, cases investigated here include 1:32 BN, 1:8 BN and 1:8 Al_2O_3 inclusion in PVdF. A case of 1:8 800 nm Al_2O_3+2.5 μm BN is also investigated, which is expected to offer enhanced thermal transport compared to a nanoparticles-only case due to the reduction in thermally resistant junctions offered by multiscale micro-nano particles [40].

2.3. Thermal transport measurements

The primary thermal property of interest for a GPE is thermal conductivity, which determines the amount of heat flux for a given temperature gradient [48]. In general, a high thermal conductivity is desired, since it minimizes temperature rise of the cell above ambient temperature. Thermal conductivity of the GPE samples is measured by a thermal constants analyzer (TPS 2200, Thermtest Inc., Canada) capable of 0.1 mK accuracy for temperature difference detection, as shown in Fig. 2(A). The repeatability of measurements by this instrument is established through repeated measurements of a standard test sample made of steel, which demonstrates a standard deviation of less than 1% between five measurements. Fig. 2(B) also shows pictures of PVdF and GPE samples used for thermal conductivity measurements. This instrument utilizes the transient plane source method [49,50]. In this method, a thin metal heater/sensor is sandwiched between two identical samples. It has been shown [49] that during transient heating, the measured temperature increase of the heater/sensor over a short period of time can be compared with an analytical model for heat diffusion in an infinite medium to determine the thermal transport properties of the sample. Briefly, the temperature rise at the sensor is given by [49,50]:

$$\Delta T(\tau) = \frac{P}{\pi^{\frac{3}{2}} ak} D(\tau) \quad (1)$$

where $\Delta T(\tau)$ is the temperature rise (°C), P is power input to the sensor, a is the radius of the sensor, k is the thermal conductivity of the sample and $D(\tau)$ is a dimensionless time function given by [49,50]:

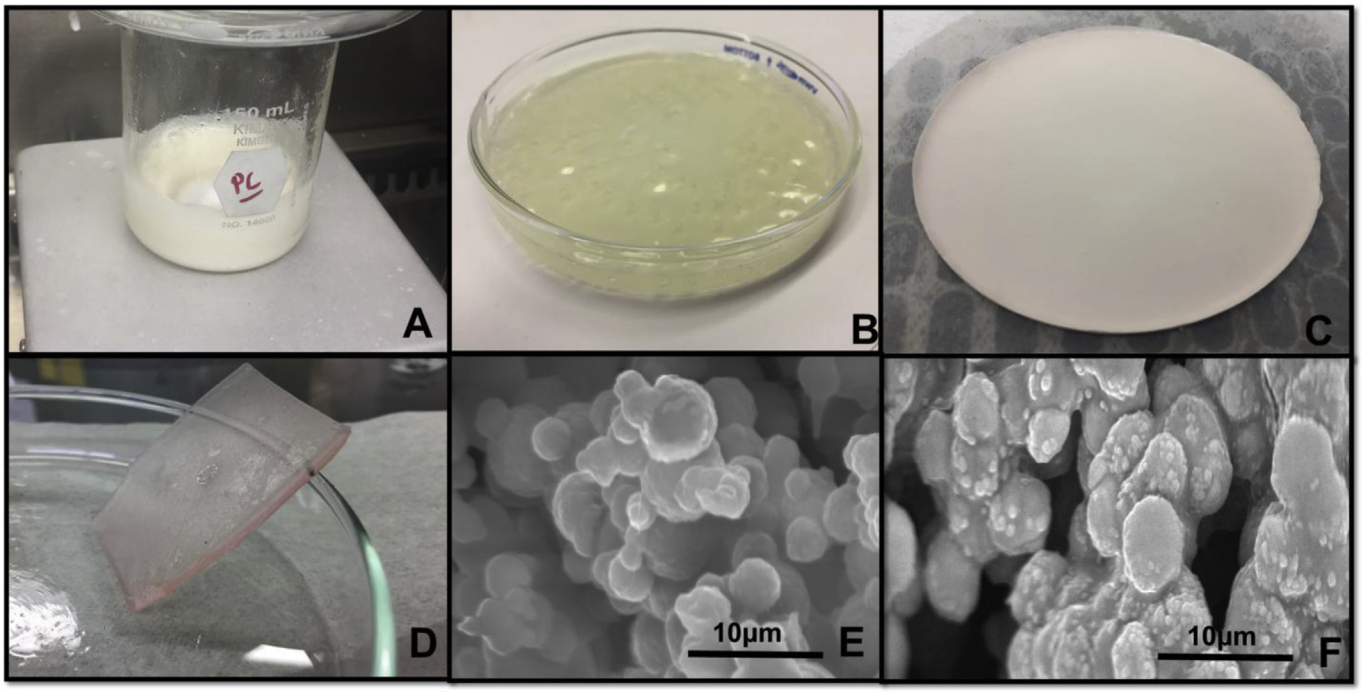

Fig. 1. Gel polymer electrolyte synthesis by casting: (A) A mixture of PVdF, EC, PC, NMP (section 2.2) is heated at 110 °C and stirred until a pale viscous solution is obtained; (B) This solution is poured in petri dishes and baked at 80 °C under 0.07 MPa vacuum in a vacuum oven for 2 h; (C) Porous PVdF membrane after soaking in 10% ethanol for 8–10 h; (D) the GPE is obtained by soaking and activating the PVdF membrane in a mixture of 1.0 M $LiPF_6$ with ionic liquid solvents; (E) SEM image of the PVdF membrane; (F) SEM image of the 800 nm BN impregnated PVdF membrane.

Table 1
Thermal conductivity (k_p) of baseline and enhanced PVdF membranes measured using the transient plane source method.

Cases	Samples	Nano/microparticles size	Weight ratio of nano/microparticles	PVdF thermal conductivity,k_p,W/mK
1A	Baseline	Nano	None	0.09 ± 0.002
1B	PVdF+BN	800nm	1:32	0.22 ± 0.004
1C	PVdF+BN	800nm	1:8	0.83 ± 0.017
1D	PVdF+Al_2O_3	800nm	1:8	0.98 ± 0.020
1E	PVdF+Al_2O_3, BN	800nm, 2.5μm	1:8	1.20 ± 0.024

Table 2
Thermal conductivity (k_{eff}) of baseline and enhanced GPE membranes measured using the transient plane source method.

Cases	Samples	Nano/microparticles size	Weight ratio of nano/microparticles	GPE thermal conductivity,k_{eff},W/mK
2A	Baseline	Nano	None	0.09 ± 0.002
2B	PVdF+BN	800nm	1:32	0.22 ± 0.004
2C	PVdF+BN	800nm	1:8	0.83 ± 0.017
2D	PVdF+Al_2O_3	800nm	1:8	0.98 ± 0.020
2E	PVdF+Al_2O_3, BN	800nm, 2.5μm	1:8	1.2 ± 0.024

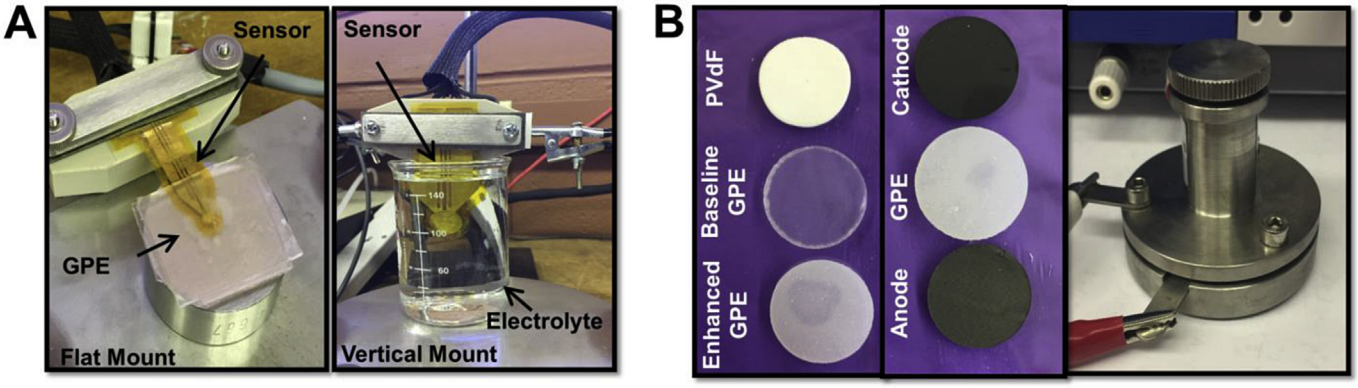

Fig. 2. (A) Pictures of experimental setup for thermal conductivity measurement on GPE and electrolyte mixture using the transient plane source method. (B) Pictures of PVdF, baseline and nanoparticle-impregnated GPE. Pictures of electrodes and GPE for single-layer cell fabrication and testing are also shown.

$$D(\tau) = \frac{1}{m^2(m+1)^2}\int_0^{\tau}\frac{d\mu}{\mu^2}\sum_{i=1}^{m} i\sum_{l=1}^{m} l e^{-((i^2+l^2)/m^2)/4\mu^2} I_0\left(\frac{il}{2m^2\mu^2}\right) \quad (2)$$

In equation (2), m refers to the number of the concentric ring sources in the heater.

Note that $\tau = \frac{\sqrt{\alpha t}}{a}$ involves the thermal diffusivity α, which is determined as the value that results in a linear relationship between the measured functions $\Delta T(\tau)$ and $D(\tau)$ based on equation (1). Following this, thermal conductivity is obtained from the slope of this relationship, as indicated by equation (1).

In these experiments, a 2.01 mm diameter heater is utilized. Due to temperature-dependent resistivity of the metal heater, it can simultaneously be used as a temperature sensor. The time period of the experiment is chosen such that it preserves the infinite medium assumption and results in highest possible sensitivity.

2.4. Electrochemical measurements

Two-probe method is used to first measure the ionic conductivity of the GPE. The ionic conductivity of the GPE is measured by EIS using two steel plates (active area ~3.14 cm^2) as the blocking electrode cells. The GPE membrane is placed between two steel plates and enclosed in a split flat cell setup (MTI Corporation), as shown in Fig. 2(B). Measurements are carried out at room temperature. Ionic conductivity is determined using measurements of internal resistance (Z), cross-section area (A) and thickness (h) of the sample as follows:

$$\sigma = \frac{h}{Z \cdot A} \quad (3)$$

Following ionic conductivity measurements, a split flat cell (MTI Corporation) with an active area of 3.14 cm^2 is utilized for electrochemical characterization of a GPE and GPE based single-layer Li-ion cell without and with micro/nanoparticle enhancement. The assembly of the cell is carried out in an inert Argon atmosphere inside a glovebox (LC Technologies). 80 μm thick $LiFePO_4$ positive electrode (MTI Corporation) and 80 μm thick graphite-based negative electrode (MTI Corporation) are assembled along with a 100 μm thick GPE. Pictures of electrodes and GPE samples used for the cell assembly process are shown in Fig. 2(B).

After cell assembly, the cell is kept at rest for 24 h for minimum potential buildup. Electrochemical Impedance Spectroscopy (EIS) experiments are conducted using a VersaSTAT4 potentiostat/galvanostat over a frequency range from 0.1 mHz to 100 MHz at open circuit with an amplitude of 10 mV while the cells are fully discharged. In order to characterize the charging and discharging performance of various GPE samples, the cells are charged at 5 mA

current up to 3.1 V, followed by discharge at the same current up to 2.2 V using the same instrument. To avoid overcharge/discharge of a cell, pre-established limits of 3.6 V for charging and 2.2 V for discharging are implemented.

3. Theoretical heat transfer model

From a heat transfer perspective, the GPE is a heterogeneous system comprising a porous PVdF matrix filled with liquid electrolyte. Several theoretical and empirical models have been proposed to predict the effective thermal conductivity of such systems [51–54]. In the past, expressions for effective thermal conductivity bounds for macroscopically homogeneous, isotropic, two-phase materials based on volume fractions and thermal conductivities of constituents have been proposed. These expressions usually utilize the Maxwell-Eucken model [55]. However, this model assumes that the inclusions of the dispersed phase, such as particles or bubbles do not come into contact with neighboring inclusions, resulting in a lack of continuous path for heat conduction by the dispersed phase. In contrast, the porous GPE samples investigated here (Supplementary Fig. S2(A)) appear to provide a continuous heat conduction path through the dispersed phase, as shown through image analysis (Supplementary Figs. S2(B)), where dark regions are the liquid electrolyte mixture and bright regions are PVdF grains. In such a case, the Effective Medium Theory (EMT) is a more appropriate model. EMT theory predicts the effective thermal conductivity, k_{eff} of a porous system as follows [51–54]:

$$k_{eff} = \frac{1}{4}\left((3v_e - 1)k_e + [3(1 - v_e) - 1]k_p + \sqrt{\left[(3v_e - 1)k_e + (3\{1 - v_e\} - 1)k_p\right]^2 + 8k_p k_e}\right) \quad (4)$$

where v_e is the volume fraction of electrolyte in the PVdF matrix, k_e and k_p are thermal conductivity of the electrolyte mixture and PVdF respectively.

4. Results and discussion

4.1. Thermal transport measurements

GPE is a binary system with liquid electrolyte immobilized within the porous PVdF matrix. Therefore, the thermal conductivity of the electrolyte plays an important role in determining the overall effective thermal conductivity of the GPE and is measured first. Fig. 2(A) shows the experimental setup for measuring thermal conductivity of the electrolyte. Instead of using a horizontal stage for mounting the transient plane source sensor, as is the usual case, a vertical stage is designed to hold and submerge the sensor head in the liquid of interest (Fig. 2(A)). A plot of the temperature rise normalized by power, $\Delta T(\tau)/P$ as a function of the dimensionless time $D(\tau)$ for the electrolyte measurement is shown in Supplementary Fig. S3. A linear relationship is found, in accordance with equation (3). Thermal conductivity of the electrolyte mixture is measured in this manner to be 0.35 ± 0.01 W/mK.

Thermal conductivity measurement of various GPE samples without and with nanoparticles is carried out next. Fig. 3 plots the sensor temperature rise normalized by power, $\Delta T(\tau)/P$, as a function of the dimensionless time $D(\tau)$ for five different cases of unactivated PVdF membrane. As discussed in section 2.3, a plot of $\Delta T(\tau)/P$ versus $D(\tau)$ is expected to be linear with thermal conductivity related to the slope M as follows:

$$k = \left(\frac{1}{\pi^{\frac{3}{2}} aM}\right) \quad (5)$$

The linear nature of $\Delta T(\tau)/P$ versus $D(\tau)$ curves as shown in Fig. 3 for each case confirms the validity of the measurement.

Thermal conductivity values for five different cases measured in this manner are summarized in Table 1 and also shown in Fig. 3. Thermal conductivity for the baseline, un-activated PVdF membrane without nanoparticle inclusion (Case 1A) is measured to be 0.09 ± 0.002 W/mK. Enhancement in thermal conductivity is observed in each case when BN or Al_2O_3 nano/microparticles are embedded. The measured enhancement is greater at higher weight ratios of the nano/microparticles, with 9X enhancement at 1:8 wt ratio. The enhancement with Al_2O_3 nanoparticles (Case 1D) is somewhat larger than with BN nanoparticles (Case 1C) for the same weight ratio. Interestingly, even further enhancement in thermal conductivity is measured when using a mixture of 800 nm Al_2O_3 nanoparticles and 2.5 μm BN microparticles (Case 1E). The measured thermal conductivity of 1.2 W/mK represents a significant, 13X improvement in thermal conductivity compared to the baseline sample (Case 1A). The observed thermal conductivity enhancement is explained well by the effective medium model as

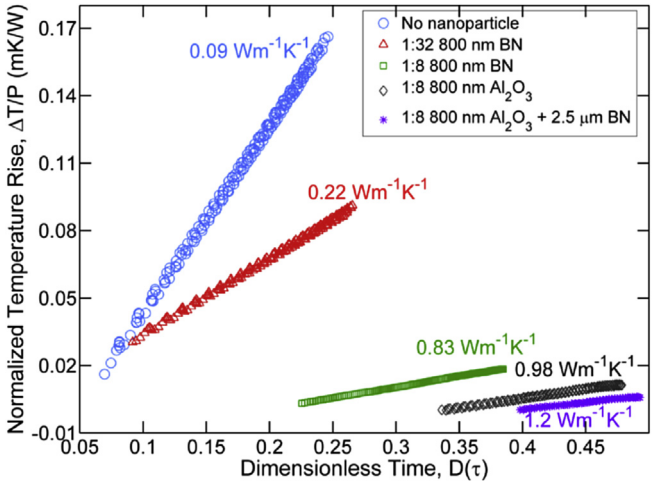

Fig. 3. Normalized temperature rise, $\Delta T/P$ as a function of dimensionless time $D(\tau)$ for thermal conductivity (k_p) measurement of baseline and thermally enhanced PVdF membranes.

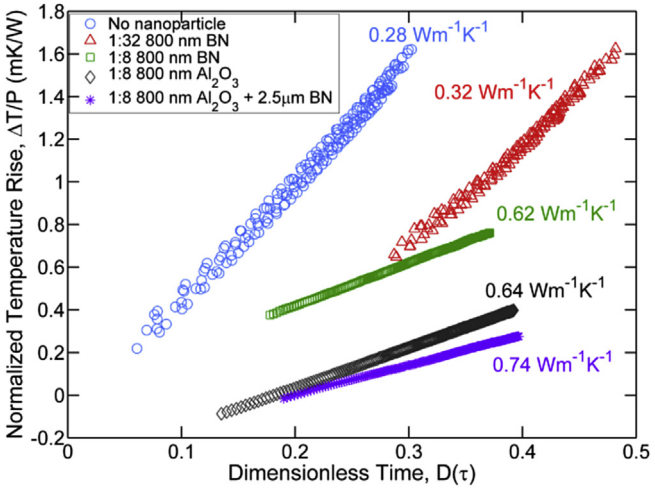

Fig. 4. Normalized temperature rise, $\Delta T/P$ as a function of dimensionless time $D(\tau)$ for thermal conductivity (k_{eff}) measurement of baseline and thermally enhanced GPE samples.

discussed later in section 4.3.

Another set of experiments are carried out to investigate the effect of nano/microparticle inclusion in the GPE formed by activating the PVdF membranes with electrolyte. Fig. 4 plots the temperature rise $\Delta T(\tau)/P$ at the sensor as a function of the dimensionless time $D(\tau)$ for these measurements, showing linear behavior for each case as expected. Measured values of thermal conductivity are shown in Fig. 4 and summarized in Table 2.

The thermal conductivity of baseline GPE (Case 2A) is measured to be 0.28 ± 0.006 W/mK, which is significantly larger than that of the unactivated PVdF membrane (Case 1A) due to increased thermal conduction by the electrolyte in the activated samples. The degree of enhancement in thermal conductivity due to nano/microparticle inclusion in GPE is somewhat lower compared to the unactivated PVdF membranes. For example, there is 2.5X enhancement with 1:8 wt ratio of a combination of Al_2O_3 nanoparticles and BN microparticles (Case 2E). Since the baseline thermal conductivity itself is so low, this 2.5X enhancement is quite significant and may result in significant reduction in peak operating temperature at large discharge rates [28], and potentially improved thermal runaway behavior. A similar enhancement is measured for 800 nm Al_2O_3 nanoparticles (Case 2D) as well. Finally, similar to experiments on unactivated PVdF membranes, there is additional enhancement when using a combination of micro and nanoparticles (Case 2E) instead of nanoparticles only. This synergistic effect is consistent with observations in past papers [32].

4.2. Electrochemical measurements

Various compositions of ionic liquids (EC:PC:EMI-TF = 0:1:1, 1:1:6, 1:1:2) in 1:1 $LiPF_6$ mixture and various percentages of ionic liquid in an electrolyte mixture have been investigated in the literature in the past [43]. In the present work, a 1:1:2 composition of EC, PC and EMI-TF is mixed in 1:1 ratio with 1 M $LiPF_6$, which has been reported to have higher ionic conductivity [43]. As shown in Fig. 5(A), the ionic conductivity of the activated GPE without any thermal enhancement is found to be 4.1 ± 0.25 mS/cm whereas ionic conductivity of the 1:8 micro/nano BN-Al_2O_3 embedded GPE (Case 2E) is found to be 1.4 ± 0.03 mS/cm. Fig. 5(B) shows the Nyquist plot for all the cases discussed in Fig. 5(A). As expected internal resistance (Z) offered by baseline sample (Case 2A) is found to be 4.2 ± 0.7 Ohms whereas internal resistance for the enhanced sample (Case 2E) is found to be 17.4 ± 0.3 Ohms. Case 2C and 2D also result in higher internal resistance due to reduced volume fraction of electrolyte mixture in the PVdF matrix resulting from micro/nano particles loading [39]. Therefore as per equation (3), increased internal resistance has resulted in reduction in ionic conductivity.

In order to further investigate the effect of thermal enhancement of the GPE on battery performance, electrochemical tests are performed in a split flat cell on a single layer cell using the GPE samples. Fig. 6(A) shows the charge discharge profile of cells with baseline, unenhanced GPE sample (Case 2A) and BN-Al_2O_3 embedded GPE (Case 2E). The two curves are similar in nature to each other. The charging potential for the enhanced GPE case is about ~44 mV lower than the traditional GPE at the peak of charging potential, until it reaches 3.1 V. However, the discharge potential of enhanced GPE is about ~140 mV higher than the traditional GPE as the discharge potential reaches lower threshold limit of 2.2 V, indicating somewhat better discharge capacity with more available energy in the thermally enhanced case. Ceramics such as Al_2O_3 and BN possess high dielectric constant, which helps in capturing anions in the liquid electrolyte and transferring lithium ions without coordinating with the anions. This could be the possible reason for the increased discharged plateau of the enhanced case.

The internal resistance of the cell is also determined by electrochemical impedance spectroscopy (EIS) measurement at fully discharged state. As shown in Fig. 6(B), the internal resistance for BN-Al_2O_3 embedded GPE based cell is found to be 6.7 Ohms which is 2 Ohms more that the unenhanced GPE based cell. Also, the diameter of the semicircle, representing the charge transfer resistance, is slightly larger for BN-Al_2O_3 embedded GPE based cell (R_2>R_1). The small increase in internal resistance and charge transfer resistance may be due to the presence of the micro/nano particles. Further, cyclic voltammogram (CV) experiments are conducted to investigate the impact of nano/micro particle inclusion in the GPE on cycling performance. Fig. 7 plots CV profiles of the GPE based Li-ion cell ($LiFePO_4$/PVdF-GPE/Li) at a scan rate of 0.5 mV/s for 1st,10th and 20th cycles, over a voltage range of 1.5–3.5 V versus Li/Li$^+$ to reveal the continual delithiation/lithiation during the charge and discharge cycles. These plots, particularly at the 10th and 20th cycles show similar characteristics of the baseline (Case 2A) and enhanced (Case 2E) samples. During the 1st cycle, both baseline and enhanced samples exhibit large reduction peak at 1.6 V and 1.7 V corresponding to reduction of $FePO_4$. Oxidation peaks for baseline and enhanced samples after the 1st cycle is around 3.2 V. Reduction and oxidation peaks for both cases shift somewhat to 1.8 V and 3.4 V respectively after the 10th and 20th cycles, indicating the polarization of electrode material in the first cycle [56]. During the 1st cycle, the CV profile of baseline (Case2A) shows higher peak than that of enhanced (Case 2E) samples, indicating more lithium ions can be reversibly stored/released [57]. However, after around 10 cycles, the values of the current peaks for baseline and enhanced samples are very close to each other, indicating that the reaction kinetics of Li$^+$ ion insertion/

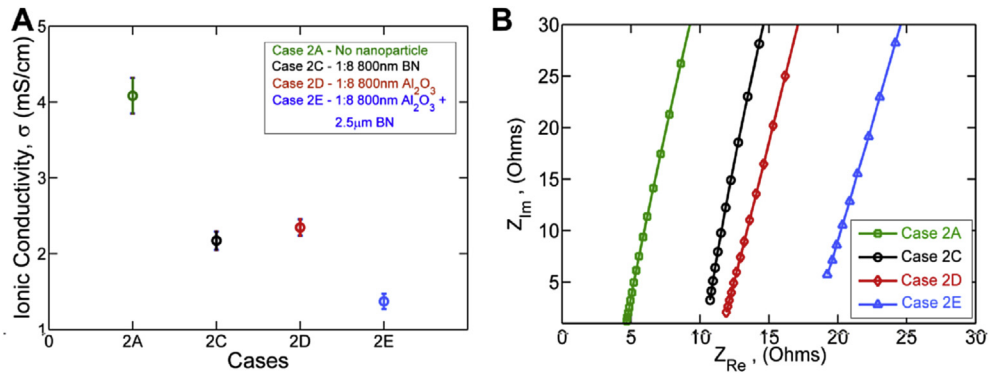

Fig. 5. (A) Ionic conductivity measurement of GPE samples with different concentrations of micro-sized (2.5 μm BN) and nano-sized (800 nm Al_2O_3) ceramic particles. (B) Nyquist plot for baseline and enhanced GPE samples (Case 2A, Case 2C, Case 2D and Case 2E) to obtain internal resistance for ionic conductivity calculation.

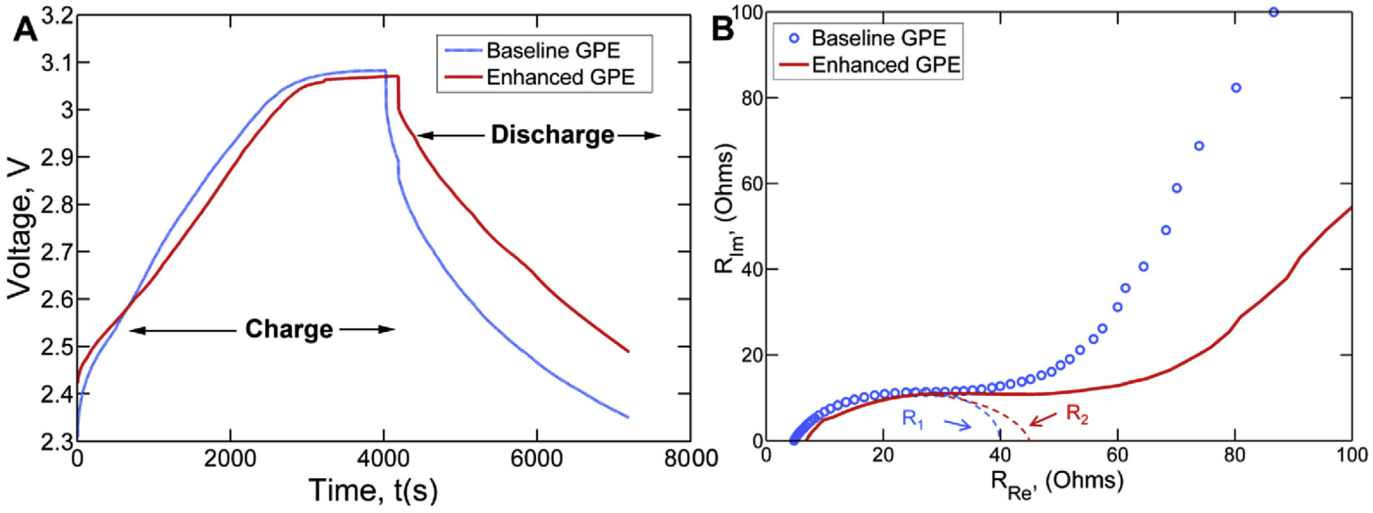

Fig. 6. Electrochemical evaluation of baseline and thermally enhanced GPEs in a half-coin cell format: (A) charge discharge performance at 5 mA, and (B) Electrochemical Impedance Spectroscopy (EIS) measured at fully discharge state.

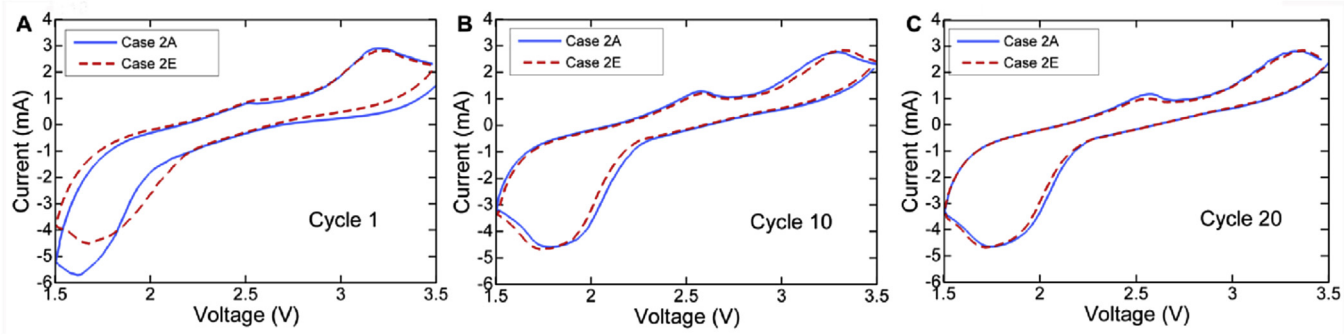

Fig. 7. Cyclic voltammetry profile of the reversible anodic and cathodic cycles for baseline (Case 2A) and enhanced (Case 2E) GPE based $LiFePO_4$/PVdF-GPE/LiC Li-ion split cell at the scan rate of 0.5 mV/s for 1st, 10th and 20th cycles.

extraction is not affected by the presence of the nano-micro particles. In summary, these measurements indicate some changes in key electrochemical characteristics due to nanoparticle inclusion that occur along with improved thermal transport. For example, the 2.5X improvement in thermal conductivity is accompanied by a 3X reduction in ionic conductivity, most likely due to the reduced volume fraction of the electrolyte due to nano/microparticle loading [38]. Such a reduction could potentially be offset with a more effective composition of the electrolyte, which has not been optimized in the present work, but is being widely investigated in other efforts [43]. At the cell level, the electrochemical performance of the thermally enhanced cell is not dramatically different from baseline cell. Nevertheless, these changes in electrochemical performance need to be recognized in conjunction with the improved thermal transport in order to appropriately balance thermal-electrochemical trade-offs in the cell.

4.3. Theoretical modeling results

The material properties and volume fraction values used for k_{eff} calculations are listed in Supplementary Table 1. The measured thermal conductivity of the micro-nanoparticles embedded PVdF membranes (k_p), presented in Table 1 are used for the calculation of effective thermal conductivity of the GPE. Thermal conductivity of electrolyte, k_e is taken to be 0.35 W/mK, based on measurements described in section 4.1. Based on equation (3), the theoretical effective thermal conductivity (k_{eff}) of the baseline GPE is calculated to be 0.24 ± 0.03 W/mK, which agrees very closely with the experimentally measured value of 0.28 ± 0.05 W/mK. Fig. 8(A) compares the theoretically computed values of k_{eff} based on the EMT model with experimental measurements for various micro/nanoparticles embedded in the GPE. In each case, experimental measurements and theory are in good agreement with each other, and are well within the estimated error bounds. Potential sources of error that may contribute towards the small deviation between the two may include error associated with volume fraction calculation, experimental uncertainties associated with measurements, etc.

Fig. 8(B) plots the theoretically calculated k_{eff} as a function of the volume fraction of the dispersed electrolyte phase. Experimentally measured values for four cases listed in Table 2 (Cases 2A, 2B, 2C and 2E) are also shown for reference. There is a good agreement between the experimental data and the model. It is interesting to note that going from Case 2B to 2E, a 20% reduction in the volume fraction of electrolyte results in more than 60% increment in the effective thermal conductivity, both experimentally measured and predicted by the model. On the other hand, incorporating higher thermal conductivity ceramic fillers at relatively lower weight fraction compared to the cases investigated here may result in simultaneous improvement in both thermal conductivity and ionic conductivity. Further optimization may be needed for selecting the

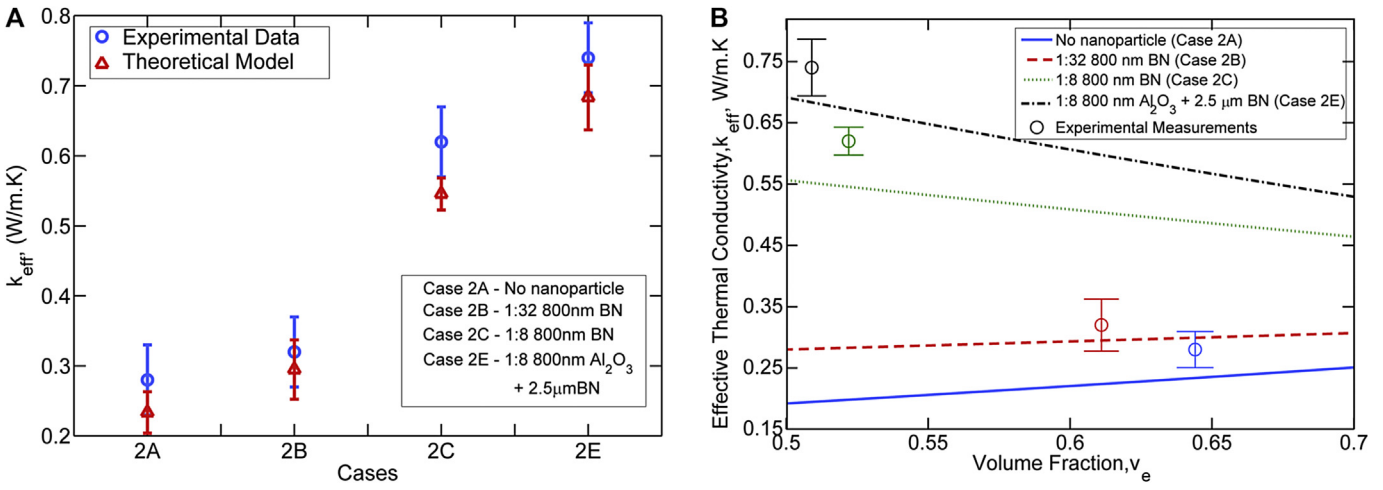

Fig. 8. (A) Comparison of experimentally measured k_{eff} of GPE samples (Table 2) with theoretical predictions based on the Effective medium theory (EMT) model. (B) Theoretically predicted variation of k_{eff} with volume fraction of electrolyte (v_e) in GPE. Experimental measurements are also shown for comparison.

right size of nanoparticles and their concentration in order to balance these thermal-electrochemical tradeoffs in a GPE based Li-ion cell.

5. Conclusions

This work presents thermal conductivity measurement and enhancement of PVdF-based GPE using BN and Al_2O_3 ceramic micro-nanoparticles. Up to 13× and 2.5× improvement in thermal conductivity is reported for PVdF membranes and GPE respectively. Since the baseline GPE has very poor thermal conductivity, this is a significant enhancement that may cause large reduction in operating temperature of GPE-based Li-ion cells, where the GPE offers the greatest thermal impedance among all materials. A theoretical understanding of the effect of nanoparticle inclusion is offered using the effective medium theory, which is found to be in good agreement with experimental measurements. The effect of such thermal enhancement on electrochemical characteristics is also investigated.

Thermal conductivity measurement and enhancement presented in this work are important for a complete understanding of thermal transport in GPE based Li-ion cells, and for designing cells with superior thermal performance. Further, these results highlight the importance of considering thermal-electrochemical tradeoffs in the design of GPE-based Li-ion cells.

Acknowledgments

This material is based upon work supported by CAREER Award No. CBET-1554183 from the National Science Foundation. The authors would like to acknowledge Prof. Fuqiang Liu for useful discussions.

Appendix A. Supplementary data

Supplementary data related to this article can be found at http://dx.doi.org/10.1016/j.jpowsour.2017.07.035.

References

[1] G. Karimi, X. Li, Thermal management of lithium-ion batteries for electric vehicles, Int. J. Energy Res. 37 (2012) 13–24.
[2] S. Jung, C. Lauterbach, M. Strasser, W. Weber, Enabling technologies for disappearing electronics in smart textiles, Proc. IEEE Int. Solid State Circ. Conf. 1 (2003) 386.
[3] L. Zhou, A. Wanga, S.C. Wu, J. Sun, S. Park, T.N. Jackson, All-organic active matrix flexible display, Appl. Phys. Lett. 88 (2006), 083502.
[4] Q. Wang, P. Ping, X. Zhao, G. Chu, J. Sun, C. Chen, Thermal runaway caused fire and explosion of lithium ion battery, J. Power Sources 208 (2012) 210–224, http://dx.doi.org/10.1016/j.jpowsour.2012.02.038.
[5] H. Maleki, Thermal stability studies of Li-Ion cells and components, J. Electrochem. Soc. 146 (1999) 3224, http://dx.doi.org/10.1149/1.1392458.
[6] W.H. Meyer, Polymer electrolytes for lithium-ion batteries, Adv. Mater 10 (1998) 439–448, http://dx.doi.org/10.1002/(SICI)1521-4095(199804)10:6<439::AID-ADMA439>3.0.CO;2-I.
[7] A.M. Stephan, Review on gel polymer electrolytes for lithium batteries, Eur. Polym. J. 42 (2006) 21–42, http://dx.doi.org/10.1016/j.eurpolymj.2005.09.017.
[8] J.Y. Song, Y.Y. Wang, C.C. Wan, Review of gel-type polymer electrolytes for lithium-ion batteries, J. Power Sources 77 (1999) 183–197, http://dx.doi.org/10.1016/S0378-7753(98)00193-1.
[9] P. Arora, Z. Zhang, Battery separators, Chem. Rev. 104 (10) (2004) 4419–4462.
[10] J.H. Cho, J. Lee, Y. Xia, B. Kim, Y. He, M.J. Renn, T.P. Lodge, C. Daniel Frisbie, Printable ion-gel gate dielectrics for low-voltage polymer thin-film transistors on plastic, Nat. Mater 7 (2008) 900–906, http://dx.doi.org/10.1038/nmat2291.
[11] C. Meng, C. Liu, L. Chen, C. Hu, S. Fan, Highly flexible and all-solid-state paperlike polymer supercapacitors, Nano Lett. 10 (2010) 4025–4031, http://dx.doi.org/10.1021/nl1019672.
[12] M. Armand, J.-M. Tarascon, Building better batteries, Nature 451 (2008) 652–657, http://dx.doi.org/10.1038/451652a.
[13] Y.S. Lee, J.H. Lee, J.A. Choi, W.Y. Yoon, D.W. Kim, Cycling characteristics of lithium powder polymer batteries assembled with composite gel polymer electrolytes and lithium powder anode, Adv. Funct. Mater 23 (2013) 1019–1027, http://dx.doi.org/10.1002/adfm.201200692.
[14] E.H. Kil, K.H. Choi, H.J. Ha, S. Xu, J.A. Rogers, M.R. Kim, Y.G. Lee, K.M. Kim, K.Y. Cho, S.Y. Lee, Imprintable, bendable, and shape-conformable polymer electrolytes for versatile-shaped lithium-ion batteries, Adv. Mater 25 (2013) 1395–1400, http://dx.doi.org/10.1002/adma.201204182.
[15] G.B. Appetecchi, F. Croce, R. Marassi, S. Panero, F. Ronci, G. Savo, B. Scrosati, Novel types of lithium-ion polymer electrolyte batteries, Solid State Ionics 143 (2001) 73–81, http://dx.doi.org/10.1016/S0167-2738(01)00835-9.
[16] C. Sirisopanaporn, A. Fernicola, B. Scrosati, New, ionic liquid-based membranes for lithium battery application, J. Power Sources 186 (2009) 490–495, http://dx.doi.org/10.1016/j.jpowsour.2008.10.036.
[17] J.H. Shin, W.A. Henderson, S. Passerini, Ionic liquids to the rescue? Overcoming the ionic conductivity limitations of polymer electrolytes, Electrochem. Commun. 5 (2003) 1016–1020, http://dx.doi.org/10.1016/j.elecom.2003.09.017.
[18] A. Kumar, S. Logapperumal, R. Sharma, M.K. Das, K.K. Kar, Li-ion transport, structural and thermal studies on lithium triflate and barium titanate incorporated poly(vinylidene fluoride-co-hexafluoropropene) based polymer electrolyte, Solid State Ionics 289 (2016) 150–158, http://dx.doi.org/10.1016/j.ssi.2016.03.008.
[19] C.M. Yang, H.S. Kim, B.K. Na, K.S. Kum, B.W. Cho, Gel-type polymer electrolytes with different types of ceramic fillers and lithium salts for lithium-ion polymer batteries, J. Power Sources 156 (2006) 574–580, http://dx.doi.org/10.1016/j.jpowsour.2005.06.018.
[20] J.B. Goodenough, Y. Kim, Challenges for rechargeable Li batteries, Chem. Mater 22 (2010) 587–603, http://dx.doi.org/10.1021/cm901452z.
[21] Y. Cui, J. Chai, H. Du, Y. Duan, G. Xie, Z. Liu, et al., Facile and reliable in Situ Polymerization of Poly(Ethyl Cyanoacrylate)-based polymer electrolytes toward flexible lithium batteries, ACS Appl. Mater. Interfaces 9 (2017) 8737–8741, http://dx.doi.org/10.1021/acsami.6b16218.

[22] J.H. Shin, W.A. Henderson, S. Scaccia, P.P. Prosini, S. Passerini, Solid-state Li/LiFePO4 polymer electrolyte batteries incorporating an ionic liquid cycled at 40 °C, J. Power Sources 156 (2006) 560–566, http://dx.doi.org/10.1016/j.jpowsour.2005.06.026.
[23] S. Sekhon, H.P. Singh, Ionic conductivity of PVdF-based polymer gel electrolytes, Solid State Ionics 152–153 (2002) 169–174, http://dx.doi.org/10.1016/S0167-2738(02)00296-5.
[24] K. Xu, Nonaqueous liquid electrolytes for lithium-based rechargeable batteries, Chem. Rev. 104 (2004) 4303–4417, http://dx.doi.org/10.1021/cr030203g.
[25] A. Fernicola, B. Scrosati, H. Ohno, Potentialities of ionic liquids as new electrolyte media in advanced electrochemical devices, Ionics (Kiel) 12 (2006) 95–102, http://dx.doi.org/10.1007/s11581-006-0023-5.
[26] M. Egashira, H. Todo, N. Yoshimoto, M. Morita, Lithium ion conduction in ionic liquid-based gel polymer electrolyte, J. Power Sources 178 (2008) 729–735, http://dx.doi.org/10.1016/j.jpowsour.2007.10.063.
[27] M. Armand, F. Endres, D.R. MacFarlane, H. Ohno, B. Scrosati, Ionic-liquid materials for the electrochemical challenges of the future, Nat. Mater 8 (2009) 621–629, http://dx.doi.org/10.1038/nmat2448.
[28] V. Vishwakarma, C. Waghela, Z. Wei, R. Prasher, S.C. Nagpure, J. Li, F. Liu, C. Daniel, A. Jain, Heat transfer enhancement in a lithium-ion cell through improved material-level thermal transport, J. Power Sources 300 (2015) 123–131, http://dx.doi.org/10.1016/j.jpowsour.2015.09.028.
[29] X.-G. Sun, Y. Fang, X. Jiang, K. Yoshii, T. Tsuda, S. Dai, Polymer gel electrolytes for application in aluminum deposition and rechargeable aluminum ion batteries, Chem. Commun. 52 (2015), http://dx.doi.org/10.1039/C5CC06643C.
[30] V. Vishwakarma, A. Jain, Measurement of in-plane thermal conductivity and heat capacity of separator in Li-ion cells using a transient DC heating method, J. Power Sources 272 (2014) 378–385, http://dx.doi.org/10.1016/j.jpowsour.2014.08.066.
[31] K. Shah, V. Vishwakarma, A. Jain, Measurement of multiscale thermal transport phenomena in li-ion cells: a review, J. Electrochem. Energy Convers. Storage 13 (2016), http://dx.doi.org/10.1115/1.4034413, 030801.
[32] Y. Yang, X. Huang, Z. Cao, G. Chen, Thermally conductive separator with hierarchical nano/microstructures for improving thermal management of batteries, Nano Energy 22 (2016) 301–309, http://dx.doi.org/10.1016/j.nanoen.2016.01.026.
[33] P.G. Bruce, B. Scrosati, J.-M. Tarascon, Nanomaterials for rechargeable lithium batteries, Angew. Chem. 47 (2008) 2930–2946, http://dx.doi.org/10.1002/anie.200702505.
[34] O. Breuer, U. Sundararaj, Big returns from small fibers: a review of polymer/carbon nanotube composites, Polym. Compos 25 (2004) 630–645, http://dx.doi.org/10.1002/pc.20058.
[35] J. Shan, H. Tenhu, Recent advances in polymer protected gold nanoparticles: synthesis, properties and applications, Chem. Commun. (Camb) (2007) 4580–4598, http://dx.doi.org/10.1039/b707740h.
[36] Z. Li, G. Su, X. Wang, D. Gao, Micro-porous P(VDF-HFP)-based polymer electrolyte filled with Al2O3 nanoparticles, Solid State Ionics 176 (2005) 1903–1908, http://dx.doi.org/10.1016/j.ssi.2005.05.006.
[37] L. Yan, Y.S. Li, C.B. Xiang, S. Xianda, Effect of nano-sized Al2O3-particle addition on PVDF ultrafiltration membrane performance, J. Memb. Sci. 276 (2006) 162–167, http://dx.doi.org/10.1016/j.jsb.2006.03.024.
[38] O. Sakarya, S. Kurama, G. Gunkaya, Effect of Al2O3 Nanofiller on ion conductivity, transmittance, and glass transition temperature of PEI: LiTFSI: PC:EC polymer electrolytes, J. Polym. Res. 24 (2016), http://dx.doi.org/10.1007/s10965-016-1172-5.
[39] K.-W. Kim, H.W. Kim, Y. Kim, J.-K. Kim, Composite gel polymer electrolyte with ceramic particles for LiNi 1/3 Mn 1/3 Co 1/3 O 2 -Li 4 Ti 5 O 12 lithium ion batteries, Electrochim. Acta 236 (2017) 394–398, http://dx.doi.org/10.1016/j.electacta.2017.03.176.
[40] H. Ishida, S. Rimdusit, Very high thermal conductivity obtained by boron nitride-filled polybenzoxazine, Thermochim. Acta 320 (1998) 177–186, http://dx.doi.org/10.1016/s0040-6031(98)00463-8.
[41] W. Zhou, S. Qi, Q. An, H. Zhao, N. Liu, Thermal conductivity of boron nitride reinforced polyethylene composites, Mater. Res. Bull. 42 (2007) 1863–1873, http://dx.doi.org/10.1016/j.materresbull.2006.11.047.
[42] G.-W. Lee, M. Park, J. Kim, J.I. Lee, H.G. Yoon, Enhanced thermal conductivity of polymer composites filled with hybrid filler, Compos. Part A Appl. Sci. Manuf. 37 (2006) 727–734, http://dx.doi.org/10.1016/j.compositesa.2005.07.006.
[43] R. Zhang, N. Hashemi, M. Ashuri, R. Montazami, in: Advanced Gel Polymer Electrolyte for Lithium-ion Polymer Batteries, ASME 2013 7th International Conference on Energy Sustainability, 2013, http://dx.doi.org/10.1115/es2013-18386.
[44] V. Gentili, S. Panero, P. Reale, B. Scrosati, Composite gel-type polymer electrolytes for advanced, rechargeable lithium batteries, J. Power Sources 170 (2007) 185–190, http://dx.doi.org/10.1016/j.jpowsour.2007.04.008.
[45] J.R. Kim, S.W. Choi, S.M. Jo, W.S. Lee, B.C. Kim, Electrospun PVdF-based fibrous polymer electrolytes for lithium ion polymer batteries, Electrochim. Acta 50 (2004) 69–75, http://dx.doi.org/10.1016/j.electacta.2004.07.014.
[46] S.S. Zhang, A review on electrolyte additives for lithium-ion batteries, J. Power Sources 162 (2006) 1379–1394, http://dx.doi.org/10.1016/j.jpowsour.2006.07.074.
[47] G.P. Pandey, S.A. Hashmi, Experimental investigations of an ionic-liquid-based, magnesium ion conducting, polymer gel electrolyte, J. Power Sources 187 (2009) 627–634, http://dx.doi.org/10.1016/j.jpowsour.2008.10.112.
[48] F.P. Incropera, D.P. Dewitt, Introduction to Heat Transfer, 3rd, Wiley Inc., 2006.
[49] S.E. Gustafsson, Transient plane source techniques for thermal conductivity and thermal diffusivity measurements of solid materials, Rev. Sci. Instrum. 62 (1991) 797–804, http://dx.doi.org/10.1063/1.1142087.
[50] S.E. Gustafsson, E. Karawacki, M.N. Khan, Transient hot-strip method for simultaneously measuring thermal conductivity and thermal diffusivity of solids and fluids, J. Phys. D Appl. Phys. 12 (1979) 1411–1421, http://dx.doi.org/10.1088/0022-3727/12/9/003.
[51] R.C. Progelhof, J.L. Throne, R.R. Ruetsch, Methods for predicting the thermal conductivity of composite systems: a review, Polym. Eng. Sci. 16 (1976) 615–625, http://dx.doi.org/10.1002/pen.760160905.
[52] D.B. Ingham, I. Pop, Transport Phenomena in Porous Media, first ed., Elsevier, 1998.
[53] R. Landauer, The electrical resistance of binary metallic mixtures, J. Appl. Phys. 23 (1952) 779–784, http://dx.doi.org/10.1063/1.1702301.
[54] S. Kirkpatrick, Percolation and conduction, Rev. Mod. Phys. 45 (1973) 574–588, http://dx.doi.org/10.1103/revmodphys.45.574.
[55] Z. Hashin, S. Shtrikman, A variational approach to the theory of the effective magnetic permeability of multiphase materials, J. Appl. Phys. 33 (1962) 3125–3131, http://dx.doi.org/10.1063/1.1728579.
[56] Z. Ju, E. Zhang, Y. Zhao, Z. Xing, Q. Zhuang, Y. Qiang, et al., One-pot hydrothermal synthesis of FeMoO4Nanocubes as an anode material for lithium-ion batteries with excellent electrochemical performance, Small 11 (2015) 4753–4761, http://dx.doi.org/10.1002/smll.201501294.
[57] R. Jiang, C. Cui, H. Ma, Using graphene nanosheets as a conductive additive to enhance the rate performance of spinel LiMn2O4 cathode material, Phys. Chem. Chem. Phys. 15 (2013) 6406, http://dx.doi.org/10.1039/c3cp44516j.